Aalto University

Aaltodoc

OPEN ACCESS

Author(s):   Hinkkanen, Marko & Repo, Anna-Kaisa & Cederholm, Mikaela & Luomi, Jorma

Title: Small-signal model for saturated deep-bar induction machines

Year: 2007

Version: Post print

Please cite the original version:

Small-Signal Model for Saturated Deep-Bar Induction Machines

Marko Hinkkanen[1], Anna-Kaisa Repo[2], Mikaela Cederholm[1], and Jorma Luomi[1]
HELSINKI UNIVERSITY OF TECHNOLOGY
[1]Power Electronics Laboratory, [2]Laboratory of Electromechanics
P.O. BOX 3000, FI-02015 TKK, Finland
Email: marko.hinkkanen@tkk.fi; anna.kaisa-repo@tkk.fi;
mikaela.cederholm@tkk.fi; jorma.luomi@tkk.fi

Acknowledgments

Keywords

≪Electrical drive≫, ≪Induction motor≫, ≪Modelling≫

Abstract

A small-signal model is presented for saturated deep-bar induction machines. Inductances are allowed to saturate as a function of their own current (or flux), and the mutual saturation effect originating mainly from closed or skewed rotor slots is also included in the model. The model fulfills the reciprocity conditions, and it can applied to parameter estimation and to the analysis and development of flux angle estimation methods. The model is applied to estimating the parameters of a 37-kW deep-bar cage-induction machine, using the data from time-stepping finite-element analysis (FEA). The proposed model fits very well to the FEA data in a wide frequency range.

1 Introduction

Induction machines are usually saturated at their normal operation points. Conventionally, the main flux is assumed to saturate as a function of the magnetising current. However, the load also has a significant influence on the main flux saturation [1, 2]. This mutual saturation originates mainly from closed or skewed rotor slots [3]. The effects of saturation on the transient behaviour are not well known. For example, the dynamic effects of saturation are usually omitted in parameter estimation methods that are based on transient behaviour. Therefore, incremental parameters may be obtained instead of the expected steady-state parameters. In addition, various flux estimation methods are based on the spatial anisotropy induced by saturation [4, 5]. Since the anisotropies depend on both the flux level and the load, they cannot generally be fixed to the position of any single flux component [6]. The small-signal impedance of a saturated machine depends on the direction of the excitation signal. This effect has been modelled for the magnetising inductance in [7], but only the dependence on the magnetising current has been included in the model. If an induction machine with closed or skewed rotor slots is studied, the model for saturation should be extended.

Another phenomenon that is usually omitted within the small-signal analysis is the skin effect of rotor bars. The skin effect is mostly relevant in the case of deep rotor bars and a double-cage structure.
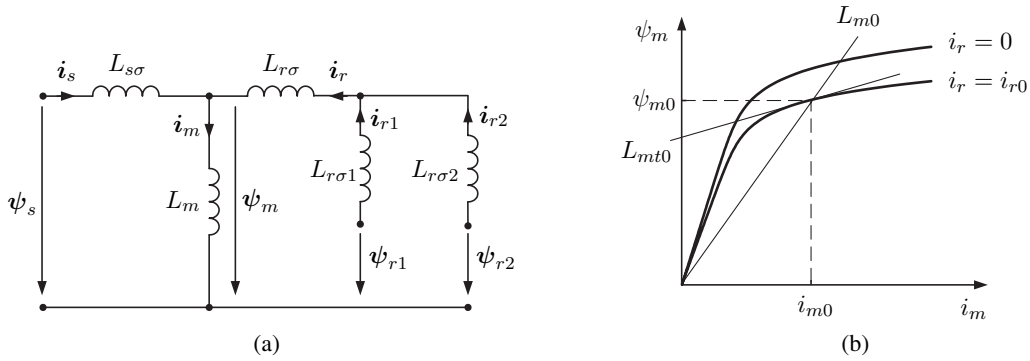
Fig. 1: (a) Model for flux linkages. (b) Typical saturation characteristics of main flux $\psi_m(i_m, i_r)$ in no-load operation ($i_r = 0$) and under load ($i_r = i_{r0}$). Steady-state magnetizing inductance $L_{m0} = \psi_{m0}/i_{m0}$ and incremental inductance $L_{mt0} = (\partial \psi_m / \partial i_m)_0$ are shown in the operating point where $i_m = i_{m0}$ and $i_r = i_{r0}$.

Typically, the skin effect has been included in large-signal circuit models by adding one or more rotor branches in parallel to the basic rotor impedance [8, 9]. The advantage of this ladder circuit model is that the values of resistances and inductances can be interpreted and evaluated based on the knowledge of rotor geometry. The number of rotor parameters may also depend on the application and the accuracy required. An alternative to the ladder circuit has been presented in [10], where the small-signal rotor impedance is represented by a high-order transfer function. The frequency-domain approach has also been used in [11], where a part of the rotor circuit is modelled as a non-integer-order system.

Both the magnetic saturation and the skin effect in the rotor bars can be modelled by the time-stepping finite-element analysis (FEA) [12]. The FEA can provide information that is difficult or even impossible to obtain by measurements. Finite-element models for electrical machines are computationally too demanding for many applications, such as comprehensive simulation models and control purposes, but the FEA can be used as a tool for providing the estimation data for small-signal model parameters. In [13], a small-signal model has been derived for deep-bar cage-induction machines, and the FEA-based numerical impulse response test has been used for parameter identification. However, the effects of saturation are not included in the model.

It is common practice to consider the losses dissipated in the magnetic circuit separately, and to use lossless inductors to model the magnetic circuit as in Fig. 1(a). The saturable magnetic circuit should fulfill the reciprocity conditions [14, 15] since otherwise the magnetic circuit may unintentionally behave as an energy source or sink. In other words, the energy stored in the magnetic circuit should be independent of the integration path. When relaxing the assumptions relating to the saturation, these conditions must be taken into account.

This paper presents a small-signal model suitable for saturated induction machines that may have closed or skewed rotor slots and deep rotor bars. Inductances are allowed to saturate as a function of their own current (or flux), and the mutual saturation effect is also included in the model. The model fulfills the reciprocity conditions. The skin effect is taken into account by an additional rotor branch, allowing the small-signal behaviour to be modelled more accurately in a wide frequency range. The applicability of the method is illustrated by estimating the parameters of a 37-kW deep-bar cage-induction machine from the data produced by FEA-based numerical impulse response tests.

2   Machine Model

Vectors will be denoted with boldface lowercase letters and matrices with boldface uppercase letters. The matrix transpose will be marked with the superscript T. The identity matrix, the orthogonal rotation

matrix, and the zero matrix are

$$\boldsymbol{I} = \begin{bmatrix} 1 & 0 \\ 0 & 1 \end{bmatrix}, \quad \boldsymbol{J} = \begin{bmatrix} 0 & -1 \\ 1 & 0 \end{bmatrix}, \quad \boldsymbol{0} = \begin{bmatrix} 0 & 0 \\ 0 & 0 \end{bmatrix} \tag{1}$$

respectively.

2.1 Large-Signal Model

In a general coordinate system rotating at angular speed ω_k, the voltage equations of the induction machine are

$$\frac{d\boldsymbol{\psi}_s}{dt} = \boldsymbol{u}_s - R_s \boldsymbol{i}_s - \omega_k \boldsymbol{J} \boldsymbol{\psi}_s \tag{2a}$$

$$\frac{d\boldsymbol{\psi}_{r1}}{dt} = \boldsymbol{u}_{r1} - R_{r1} \boldsymbol{i}_{r1} - (\omega_k - \omega_m) \boldsymbol{J} \boldsymbol{\psi}_{r1} \tag{2b}$$

$$\frac{d\boldsymbol{\psi}_{r2}}{dt} = \boldsymbol{u}_{r2} - R_{r2} \boldsymbol{i}_{r2} - (\omega_k - \omega_m) \boldsymbol{J} \boldsymbol{\psi}_{r2} \tag{2c}$$

where $\boldsymbol{u}_s = [u_{sd}, u_{sq}]^T$ is the stator voltage vector, $\boldsymbol{i}_s = [i_{sd}, i_{sq}]^T$ the stator current vector, and R_s the stator resistance. The rotor resistances are R_{r1} and R_{r2}, the rotor voltage vectors are $\boldsymbol{u}_{r1}$ and $\boldsymbol{u}_{r2}$, the rotor current vectors are $\boldsymbol{i}_{r1}$ and $\boldsymbol{i}_{r2}$, and the electrical angular speed of the rotor is ω_m.

The flux linkage vectors are

$$\boldsymbol{\psi}_s = L_s \boldsymbol{i}_s + L_m \boldsymbol{i}_{r1} + L_m \boldsymbol{i}_{r2} \tag{3a}$$

$$\boldsymbol{\psi}_{r1} = L_m \boldsymbol{i}_s + L_{r1} \boldsymbol{i}_{r1} + L_r \boldsymbol{i}_{r2} \tag{3b}$$

$$\boldsymbol{\psi}_{r2} = L_m \boldsymbol{i}_s + L_r \boldsymbol{i}_{r1} + L_{r2} \boldsymbol{i}_{r2} \tag{3c}$$

where L_m is the magnetizing inductance. Other inductances are defined by

$$L_s = L_m + L_{s\sigma}, \quad L_r = L_m + L_{r\sigma}, \quad L_{r1} = L_r + L_{r\sigma 1}, \quad L_{r2} = L_r + L_{r\sigma 2} \tag{4}$$

where $L_{s\sigma}$, $L_{r\sigma}$, $L_{r\sigma 1}$, and $L_{r\sigma 2}$ correspond to the flux linkage model in Fig. 1(a). The main flux and the leakage fluxes are

$$\boldsymbol{\psi}_m = L_m \boldsymbol{i}_m, \quad \boldsymbol{\psi}_{s\sigma} = L_{s\sigma} \boldsymbol{i}_s, \quad \boldsymbol{\psi}_{r\sigma} = L_{r\sigma} \boldsymbol{i}_r, \quad \boldsymbol{\psi}_{r\sigma 1} = L_{r\sigma 1} \boldsymbol{i}_{r1}, \quad \boldsymbol{\psi}_{r\sigma 2} = L_{r\sigma 2} \boldsymbol{i}_{r2} \tag{5}$$

where $\boldsymbol{i}_r = \boldsymbol{i}_{r1} + \boldsymbol{i}_{r2}$ is the total rotor current and $\boldsymbol{i}_m = \boldsymbol{i}_s + \boldsymbol{i}_r$ is the magnetizing current. Inductances are allowed to depend on the currents (or the fluxes), and they are assumed to be lossless.

2.2 Power Balance

For per-unit quantities, the power balance is obtained from (2) as

$$\boldsymbol{i}_s^T \boldsymbol{u}_s + \boldsymbol{i}_{r1}^T \boldsymbol{u}_{r1} + \boldsymbol{i}_{r2}^T \boldsymbol{u}_{r2} = R_s i_s^2 + R_{r1} i_{r1}^2 + R_{r2} i_{r2}^2 + \frac{dW_f}{dt} + T_e \omega_m \tag{6}$$

where $i_s = ||\boldsymbol{i}_s||$, and the magnitudes of other vectors are obtained similarly. The electromagnetic torque is

$$T_e = \boldsymbol{i}_s^T \boldsymbol{J} \boldsymbol{\psi}_s \tag{7}$$

and the rate of change of the magnetic energy is

$$\begin{aligned}
\frac{dW_f}{dt} &= \boldsymbol{i}_s^T \frac{d\boldsymbol{\psi}_s}{dt} + \boldsymbol{i}_{r1}^T \frac{d\boldsymbol{\psi}_{r1}}{dt} + \boldsymbol{i}_{r2}^T \frac{d\boldsymbol{\psi}_{r2}}{dt} \\
&= i_s \frac{d\psi_{s\sigma}}{dt} + i_m \frac{d\psi_m}{dt} + i_r \frac{d\psi_{r\sigma}}{dt} + i_{r1} \frac{d\psi_{r\sigma 1}}{dt} + i_{r2} \frac{d\psi_{r\sigma 2}}{dt}
\end{aligned} \tag{8}$$

The last form is obtained by assuming the flux vectors to be parallel with the corresponding current vectors in accordance with Fig. 1(a), while the inductances may be functions of the currents or fluxes. Based on (8), the incremental inductances should fulfill the reciprocity conditions:

$$\frac{\partial \psi_{s\sigma}}{\partial i_m} = \frac{\partial \psi_m}{\partial i_s}; \quad \frac{\partial \psi_{s\sigma}}{\partial i_r} = \frac{\partial \psi_{r\sigma}}{\partial i_s}; \quad \frac{\partial \psi_{s\sigma}}{\partial i_{r1}} = \frac{\partial \psi_{r\sigma1}}{\partial i_s}; \quad \frac{\partial \psi_{s\sigma}}{\partial i_{r2}} = \frac{\partial \psi_{r\sigma2}}{\partial i_s}; \quad \frac{\partial \psi_m}{\partial i_r} = \frac{\partial \psi_{r\sigma}}{\partial i_m} \quad (9)$$

$$\frac{\partial \psi_m}{\partial i_{r1}} = \frac{\partial \psi_{r\sigma1}}{\partial i_m}; \quad \frac{\partial \psi_m}{\partial i_{r2}} = \frac{\partial \psi_{r\sigma2}}{\partial i_m}; \quad \frac{\partial \psi_{r\sigma}}{\partial i_{r1}} = \frac{\partial \psi_{r\sigma1}}{\partial i_r}; \quad \frac{\partial \psi_{r\sigma}}{\partial i_{r2}} = \frac{\partial \psi_{r\sigma2}}{\partial i_r}; \quad \frac{\partial \psi_{r\sigma1}}{\partial i_{r2}} = \frac{\partial \psi_{r\sigma2}}{\partial i_{r1}}$$

More generally, the magnetic coupling can be modeled as a multi-terminal (or multi-port) inductor. If a flux-controlled or current-controlled inductor is lossless, it is reciprocal [14]. The incremental inductance matrix associated with a reciprocal multi-terminal inductor is symmetric.

2.3 Assumptions on Magnetic Saturation

In the following, $L_{s\sigma}$, $L_{r\sigma1}$, and $L_{r\sigma2}$ are assumed constant for simplicity, but

$$L_m(i_m, i_r) = \frac{\psi_m(i_m, i_r)}{i_m}, \quad L_{r\sigma}(i_m, i_r) = \frac{\psi_{r\sigma}(i_m, i_r)}{i_r} \quad (10)$$

cf. illustration in Fig. 1(b) relating to L_m. The following incremental inductances fulfilling (9) are defined:

$$L_{mt} = \frac{\partial \psi_m}{\partial i_m}; \quad L_{r\sigma t} = \frac{\partial \psi_{r\sigma}}{\partial i_r}; \quad L_t = \frac{\partial \psi_m}{\partial i_r} = \frac{\partial \psi_{r\sigma}}{\partial i_m} \quad (11)$$

Assuming the magnetizing current i_m constant, the main flux ψ_m decreases as the rotor current i_r increases. Hence, the incremental mutual inductance L_t is usually negative. If needed, the saturation of $L_{s\sigma}$, $L_{r\sigma1}$, and $L_{r\sigma2}$ could be easily taken into account.

3 Linearized Model

3.1 Preliminaries

In the following, a tilde refers to the deviation about the operating point, and operating-point quantities are marked with the subscript 0, e.g., $\tilde{\boldsymbol{u}}_s = \boldsymbol{u}_s - \boldsymbol{u}_{s0}$. Synchronous coordinates rotating at constant angular speed $\omega_k = \omega_{s0}$ are considered. The linearized voltage equations are

$$\frac{d\tilde{\boldsymbol{\psi}}_s}{dt} = \tilde{\boldsymbol{u}}_s - R_s \tilde{\boldsymbol{i}}_s - \omega_{s0} \boldsymbol{J} \tilde{\boldsymbol{\psi}}_s \quad (12a)$$

$$\frac{d\tilde{\boldsymbol{\psi}}_{r1}}{dt} = \tilde{\boldsymbol{u}}_{r1} - R_{r1} \tilde{\boldsymbol{i}}_r - \omega_{r0} \boldsymbol{J} \tilde{\boldsymbol{\psi}}_{r1} + \boldsymbol{J} \boldsymbol{\psi}_{r10} \tilde{\omega}_m \quad (12b)$$

$$\frac{d\tilde{\boldsymbol{\psi}}_{r2}}{dt} = \tilde{\boldsymbol{u}}_{r2} - R_{r2} \tilde{\boldsymbol{i}}_{r2} - \omega_{r0} \boldsymbol{J} \tilde{\boldsymbol{\psi}}_{r2} + \boldsymbol{J} \boldsymbol{\psi}_{r20} \tilde{\omega}_m \quad (12c)$$

where the operating-point slip angular frequency is $\omega_{r0} = \omega_{s0} - \omega_{m0}$. The deviations of the stator and rotor fluxes are

$$\tilde{\boldsymbol{\psi}}_s = L_{s0} \tilde{\boldsymbol{i}}_s + L_{m0} \tilde{\boldsymbol{i}}_{r1} + L_{m0} \tilde{\boldsymbol{i}}_{r2} + \boldsymbol{i}_{m0} \tilde{L}_m \quad (13a)$$

$$\tilde{\boldsymbol{\psi}}_{r1} = L_{m0} \tilde{\boldsymbol{i}}_s + L_{r10} \tilde{\boldsymbol{i}}_{r1} + L_{r0} \tilde{\boldsymbol{i}}_{r2} + \boldsymbol{i}_{m0} \tilde{L}_m + \boldsymbol{i}_{r0} \tilde{L}_{r\sigma} \quad (13b)$$

$$\tilde{\boldsymbol{\psi}}_{r2} = L_{m0} \tilde{\boldsymbol{i}}_s + L_{r0} \tilde{\boldsymbol{i}}_{r1} + L_{r20} \tilde{\boldsymbol{i}}_{r2} + \boldsymbol{i}_{m0} \tilde{L}_m + \boldsymbol{i}_{r0} \tilde{L}_{r\sigma} \quad (13c)$$

respectively. The linearized torque expression is

$$\tilde{T}_e = \boldsymbol{i}_{s0}^T \boldsymbol{J} \tilde{\boldsymbol{\psi}}_s - \boldsymbol{\psi}_{s0}^T \boldsymbol{J} \tilde{\boldsymbol{i}}_s \quad (14)$$

The deviation of the magnetizing inductance can be written as

$$\tilde{L}_m = \left(\frac{\partial L_m}{\partial i_m}\frac{\partial i_m}{\partial i_{md}}\right)_0 \tilde{i}_{md} + \left(\frac{\partial L_m}{\partial i_m}\frac{\partial i_m}{\partial i_{mq}}\right)_0 \tilde{i}_{mq}$$
$$+ \left(\frac{\partial L_m}{\partial i_r}\frac{\partial i_r}{\partial i_{rd}}\right)_0 \tilde{i}_{rd} + \left(\frac{\partial L_m}{\partial i_r}\frac{\partial i_r}{\partial i_{rq}}\right)_0 \tilde{i}_{rq} \tag{15}$$
$$= \frac{L_{mt0} - L_{m0}}{i_{m0}^2}\boldsymbol{i}_{m0}^T \tilde{\boldsymbol{i}}_m + \frac{L_{t0}}{i_{m0}i_{r0}}\boldsymbol{i}_{r0}^T \tilde{\boldsymbol{i}}_r$$

where $\tilde{\boldsymbol{i}}_m = \tilde{\boldsymbol{i}}_s + \tilde{\boldsymbol{i}}_r$. If no mutual saturation effect is present, i.e. $L_{t0} = 0$, the deviation $\tilde{L}_m$ of the magnetizing inductance is zero if the current deviation $\tilde{\boldsymbol{i}}_m$ is perpendicular to the operating point current $\boldsymbol{i}_{m0}$. The deviation of the rotor leakage inductance $\tilde{L}_{r\sigma}$ can be derived in a fashion similar to (15).

3.2   State-Space Representation

The deviations of the inductances $\tilde{L}_m$ and $\tilde{L}_{r\sigma}$ can be inserted into (13). Furthermore, $\tilde{\boldsymbol{i}}_s$ and $\tilde{\boldsymbol{i}}_r$ can be solved from (13) and inserted into (12), leading to a linear multiple-input state-space representation

$$\frac{d\tilde{\boldsymbol{x}}}{dt} = \boldsymbol{A}\tilde{\boldsymbol{x}} + \boldsymbol{B}_s\tilde{\boldsymbol{u}}_s + \boldsymbol{B}_{r1}\tilde{\boldsymbol{u}}_{r1} + \boldsymbol{B}_{r2}\tilde{\boldsymbol{u}}_{r2} + \boldsymbol{b}\tilde{\omega}_m \tag{16}$$

where the state vector and the input matrices are

$$\tilde{\boldsymbol{x}} = \begin{bmatrix} \tilde{\boldsymbol{\psi}}_s \\ \tilde{\boldsymbol{\psi}}_{r1} \\ \tilde{\boldsymbol{\psi}}_{r2} \end{bmatrix}, \quad \boldsymbol{B}_s = \begin{bmatrix} \boldsymbol{I} \\ \boldsymbol{0} \\ \boldsymbol{0} \end{bmatrix}, \quad \boldsymbol{B}_{r1} = \begin{bmatrix} \boldsymbol{0} \\ \boldsymbol{I} \\ \boldsymbol{0} \end{bmatrix}, \quad \boldsymbol{B}_{r2} = \begin{bmatrix} \boldsymbol{0} \\ \boldsymbol{0} \\ \boldsymbol{I} \end{bmatrix}, \quad \boldsymbol{b} = \begin{bmatrix} \boldsymbol{0} \\ \boldsymbol{J}\boldsymbol{\psi}_{r10} \\ \boldsymbol{J}\boldsymbol{\psi}_{r20} \end{bmatrix} \tag{17}$$

The state matrix is

$$\boldsymbol{A} = -\begin{bmatrix} R_s\boldsymbol{I} & \boldsymbol{0} & \boldsymbol{0} \\ \boldsymbol{0} & R_{r1}\boldsymbol{I} & \boldsymbol{0} \\ \boldsymbol{0} & \boldsymbol{0} & R_{r2}\boldsymbol{I} \end{bmatrix}\boldsymbol{L}^{-1} - \begin{bmatrix} \omega_{s0}\boldsymbol{J} & \boldsymbol{0} & \boldsymbol{0} \\ \boldsymbol{0} & \omega_{r0}\boldsymbol{J} & \boldsymbol{0} \\ \boldsymbol{0} & \boldsymbol{0} & \omega_{r0}\boldsymbol{J} \end{bmatrix} \tag{18}$$

where the inductance matrix is defined as

$$\boldsymbol{L} = \begin{bmatrix} L_{s0}\boldsymbol{I} & L_{m0}\boldsymbol{I} & L_{m0}\boldsymbol{I} \\ L_{m0}\boldsymbol{I} & L_{r10}\boldsymbol{I} & L_{r0}\boldsymbol{I} \\ L_{m0}\boldsymbol{I} & L_{r0}\boldsymbol{I} & L_{r20}\boldsymbol{I} \end{bmatrix} + \frac{L_{mt0} - L_{m0}}{i_{m0}^2}\begin{bmatrix} \boldsymbol{i}_{m0}\boldsymbol{i}_{m0}^T & \boldsymbol{i}_{m0}\boldsymbol{i}_{m0}^T & \boldsymbol{i}_{m0}\boldsymbol{i}_{m0}^T \\ \boldsymbol{i}_{m0}\boldsymbol{i}_{m0}^T & \boldsymbol{i}_{m0}\boldsymbol{i}_{m0}^T & \boldsymbol{i}_{m0}\boldsymbol{i}_{m0}^T \\ \boldsymbol{i}_{m0}\boldsymbol{i}_{m0}^T & \boldsymbol{i}_{m0}\boldsymbol{i}_{m0}^T & \boldsymbol{i}_{m0}\boldsymbol{i}_{m0}^T \end{bmatrix}$$
$$+ \frac{L_{r\sigma t0} - L_{r\sigma 0}}{i_{r0}^2}\begin{bmatrix} \boldsymbol{0} & \boldsymbol{0} & \boldsymbol{0} \\ \boldsymbol{0} & \boldsymbol{i}_{r0}\boldsymbol{i}_{r0}^T & \boldsymbol{i}_{r0}\boldsymbol{i}_{r0}^T \\ \boldsymbol{0} & \boldsymbol{i}_{r0}\boldsymbol{i}_{r0}^T & \boldsymbol{i}_{r0}\boldsymbol{i}_{r0}^T \end{bmatrix} + \frac{L_{t0}}{i_{m0}i_{r0}}\begin{bmatrix} \boldsymbol{0} & \boldsymbol{i}_{m0}\boldsymbol{i}_{r0}^T & \boldsymbol{i}_{m0}\boldsymbol{i}_{r0}^T \\ \boldsymbol{i}_{r0}\boldsymbol{i}_{m0}^T & \boldsymbol{i}_{m0}\boldsymbol{i}_{r0}^T + \boldsymbol{i}_{r0}\boldsymbol{i}_{m0}^T & \boldsymbol{i}_{m0}\boldsymbol{i}_{r0}^T + \boldsymbol{i}_{r0}\boldsymbol{i}_{m0}^T \\ \boldsymbol{i}_{r0}\boldsymbol{i}_{m0}^T & \boldsymbol{i}_{m0}\boldsymbol{i}_{r0}^T + \boldsymbol{i}_{r0}\boldsymbol{i}_{m0}^T & \boldsymbol{i}_{m0}\boldsymbol{i}_{r0}^T + \boldsymbol{i}_{r0}\boldsymbol{i}_{m0}^T \end{bmatrix} \tag{19}$$

The matrix $\boldsymbol{L}$ is symmetric due to the reciprocity conditions, and its last three terms originate from saturation.

Here, the stator current, the rotor currents, and the torque are chosen as output variables,

$$\tilde{\boldsymbol{i}}_s = \boldsymbol{C}_s\tilde{\boldsymbol{x}}, \quad \tilde{\boldsymbol{i}}_{r1} = \boldsymbol{C}_{r1}\tilde{\boldsymbol{x}}, \quad \tilde{\boldsymbol{i}}_{r2} = \boldsymbol{C}_{r2}\tilde{\boldsymbol{x}}, \quad \tilde{T}_e = \boldsymbol{c}\tilde{\boldsymbol{x}} \tag{20}$$

where the output matrices relating to the currents are

$$\boldsymbol{C}_s = \begin{bmatrix} \boldsymbol{I} & \boldsymbol{0} & \boldsymbol{0} \end{bmatrix}\boldsymbol{L}^{-1}, \quad \boldsymbol{C}_{r1} = \begin{bmatrix} \boldsymbol{0} & \boldsymbol{I} & \boldsymbol{0} \end{bmatrix}\boldsymbol{L}^{-1}, \quad \boldsymbol{C}_{r2} = \begin{bmatrix} \boldsymbol{0} & \boldsymbol{0} & \boldsymbol{I} \end{bmatrix}\boldsymbol{L}^{-1} \tag{21}$$

and the output matrix relating to the torque is

$$\boldsymbol{c} = \boldsymbol{i}_{s0}^T\begin{bmatrix} \boldsymbol{J} & \boldsymbol{0} & \boldsymbol{0} \end{bmatrix} - \boldsymbol{\psi}_{s0}^T\begin{bmatrix} \boldsymbol{J} & \boldsymbol{0} & \boldsymbol{0} \end{bmatrix}\boldsymbol{L}^{-1} \tag{22}$$

in accordance with (14). The system can easily be analyzed using conventional tools for linear systems. If the saturation is not taken into account (i.e. $L_{mt0} = L_{m0}$, $L_{r\sigma t0} = L_{r\sigma 0}$, and $L_{t0} = 0$), the small-signal model equals the conventional space-vector model of the double-cage induction machine.

3.3 Steady-State Relations

From (2) and (3), the steady-state condition

$$
\begin{bmatrix} \boldsymbol{u}_{s0} \\ \boldsymbol{u}_{r10} \\ \boldsymbol{u}_{r20} \end{bmatrix} = \begin{bmatrix} R_s\boldsymbol{I} + \omega_{s0}L_{s0}\boldsymbol{J} & \omega_{s0}L_{m0}\boldsymbol{J} & \omega_{s0}L_{m0}\boldsymbol{J} \\ \omega_{r0}L_{m0}\boldsymbol{J} & R_{r1}\boldsymbol{I} + \omega_{r0}L_{r10}\boldsymbol{J} & \omega_{r0}L_{r0}\boldsymbol{J} \\ \omega_{r0}L_{m0}\boldsymbol{J} & \omega_{r0}L_{r0}\boldsymbol{J} & R_{r2}\boldsymbol{I} + \omega_{r0}L_{r20}\boldsymbol{J} \end{bmatrix} \begin{bmatrix} \boldsymbol{i}_{s0} \\ \boldsymbol{i}_{r10} \\ \boldsymbol{i}_{r20} \end{bmatrix} \tag{23}
$$

is obtained. The operating-point voltages can thus be determined if the parameters and the operating-point currents are known.

In many applications, the stator voltage $\boldsymbol{u}_{s0}$, the stator current $\boldsymbol{i}_{s0}$, and the stator angular frequency ω_{s0} are known in the operating point. Furthermore, the rotor windings are typically short-circuited, $\boldsymbol{u}_{r10} = \boldsymbol{u}_{r20} = [0,0]^T$, while the rotor currents are inaccessible. Therefore, it is useful to solve the rotor currents from (23), i.e.

$$
\boldsymbol{i}_{r0} = \boldsymbol{i}_{r10} + \boldsymbol{i}_{r20} = -\boldsymbol{J}\left[\boldsymbol{u}_{s0} - (R_s\boldsymbol{I} + \omega_{s0}L_{s0}\boldsymbol{J})\boldsymbol{i}_{s0}\right]/(\omega_{s0}L_{m0}) \tag{24a}
$$

$$
\boldsymbol{i}_{r10} = \left[R_{r1}\boldsymbol{I} + \omega_{r0}(L_{r10} - L_{r0})\boldsymbol{J}\right]^{-1}\left[\boldsymbol{u}_{r10} - \omega_{r0}\left(L_{m0}\boldsymbol{J}\boldsymbol{i}_{s0} + L_{r0}\boldsymbol{J}\boldsymbol{i}_{r0}\right)\right] \tag{24b}
$$

Hence, the magnetizing current $\boldsymbol{i}_{m0} = \boldsymbol{i}_{s0} + \boldsymbol{i}_{r0}$ and the operating-point fluxes needed in the linearized model can be calculated. In addition to the rotor currents, two parameters can be solved from (23). Convenient choices are the rotor resistance and the rotor inductance of one cage:

$$
R_{r2} = \boldsymbol{i}_{r20}^T\left[\boldsymbol{u}_{r20} - \omega_{r0}(L_{m0}\boldsymbol{J}\boldsymbol{i}_{s0} + L_{r0}\boldsymbol{J}\boldsymbol{i}_{r10})\right]/i_{r20}^2 \tag{25}
$$

$$
L_{r20} = -\boldsymbol{i}_{r20}^T\boldsymbol{J}\left[\boldsymbol{u}_{r20} - \omega_{r0}(L_{m0}\boldsymbol{J}\boldsymbol{i}_{s0} + L_{r0}\boldsymbol{J}\boldsymbol{i}_{r10})\right]/(\omega_{r0}i_{r20}^2) \tag{26}
$$

If the linearized model is used for parameter estimation or fitting, the information in (23) should be used to avoid inconsistency with the operating-point data. Furthermore, since the number of independent parameters decreases, the fitting procedure becomes easier.

3.4 Transfer Functions

The stator current can be expressed as $\tilde{\boldsymbol{i}}_s(s) = \boldsymbol{Y}_s(s)\tilde{\boldsymbol{u}}_s(s)$, where the multiple-input-multiple-output transfer function matrix (or small-signal admittance matrix) is

$$
\boldsymbol{Y}_s(s) = \boldsymbol{C}_s\left(s\boldsymbol{I}_6 - \boldsymbol{A}\right)^{-1}\boldsymbol{B}_s \tag{27}
$$

where $\boldsymbol{I}_6$ is a 6×6 identity matrix. The expression (27) is valid in any synchronous coordinates. An admittance matrix $\boldsymbol{Y}_s'$ can be transformed to new synchronous coordinates as

$$
\boldsymbol{Y}_s(s) = e^{\vartheta_0\boldsymbol{J}}\boldsymbol{Y}_s'(s)e^{-\vartheta_0\boldsymbol{J}} \tag{28}
$$

where ϑ_0 is the angle of the d axis of original coordinates in new coordinates. The coordinate transformation matrix can be expressed as $e^{\vartheta_0\boldsymbol{J}} = \cos(\vartheta_0)\boldsymbol{I} + \sin(\vartheta_0)\boldsymbol{J}$. In the case of no saturation, $\boldsymbol{Y}_s(s) = Y_{s11}(s)\boldsymbol{I} + Y_{s21}(s)\boldsymbol{J} = \boldsymbol{Y}_s'(s)$ holds, and the admittance matrix does not depend on the angle ϑ_0. In the unsaturated case, the system could be expressed as a complex-valued single-input-single-output transfer function for complex-valued space vectors.

If torsional dynamics are of interest [16, 17], the transfer function from the rotor speed to the electromagnetic torque is needed. The electromagnetic torque can be expressed as $\tilde{T}_e(s) = G(s)\tilde{\omega}_m(s)$, where the single-input-single-output transfer function is

$$
G(s) = \boldsymbol{c}\left(s\boldsymbol{I}_6 - \boldsymbol{A}\right)^{-1}\boldsymbol{b} \tag{29}
$$

In a fashion similar to (27) and (29), other transfer-function matrices can be easily obtained using (16) and (20).

Fig. 2: Cross-section of a rotor bar. Diameter of the rotor is 198 mm and height of the rotor slot is 35 mm.

4   Results

Parameters of a 37-kW squirrel-cage induction machine were estimated using the numerical impulse response test [13, 18] based on the data obtained from time-stepping FEA [12]. The machine is equipped with deep rotor bars and closed rotor slots; the cross-section of a rotor bar is shown in Fig. 2. The rating of the machine is: voltage 380 V; current 73 A; frequency 50 Hz; and speed 1470 r/min. The base values are: angular frequency $2\pi 50$ rad/s; voltage $\sqrt{2/3} \cdot 380$ V; and current $\sqrt{2} \cdot 73$ A. The rated operating point is considered in the following.

First, the impulse excitation was applied to the three-phase supply voltage and the response of stator current was studied. Within the voltage impulse test, the rotor speed was constant. The impulse test was performed twice with perpendicular impulses: the impulse was first applied to $\tilde{u}_{sd}$ while $\tilde{u}_{sq} = 0$, and the second impulse was applied to $\tilde{u}_{sq}$ while $\tilde{u}_{sd} = 0$; the coordinates were fixed to the operating-point stator voltage. The results of time-stepping computations were transformed to the frequency domain using DFT. Since two impulse tests were made, it was possible to calculate all four admittances $Y_{s11}(j\omega)$, $Y_{s12}(j\omega)$, $Y_{s21}(j\omega)$, and $Y_{s22}(j\omega)$. The circles and crosses in Fig. 3 show the admittances from the FEA data in the coordinate system fixed to the operating-point stator voltage. If the machine were not saturated, the circles and crosses would overlap.

The admittance matrix (27) of the proposed model was fitted to the frequency-response data obtained from time-stepping FEA. The fitting was based on differential evolution [19], but other optimization methods could be used as well. To decrease the number of parameters to be fitted, $L_{s\sigma} = 0$ and $L_{r\sigma 10} = 0$ were fixed [20]. The inductances L_{m0}, $L_{r\sigma 0}$, L_{mt0}, $L_{r\sigma t0}$, and L_{t0} and the resistances R_s and R_{r1} were allowed to vary freely in the data fitting. These parameters together with the operating-point data ($\boldsymbol{u}_{s0}$, $\boldsymbol{i}_{s0}$, ω_{s0}, and ω_{r0}) obtained from FEA were used to calculate the operating-point rotor currents from (24) as well as R_{r2} from (25) and $L_{r\sigma 20} = L_{r20} - L_{m0} - L_{r\sigma 0}$ from (26). An estimate of the admittance matrix can thus be calculated according to (27). The cost function used in the data fitting is calculated as the sum of the square errors of the elements in the admittance matrix. The result of the data fitting are presented in Fig. 3. As can be seen, the model fits rather well to the data.

Table I gives the parameters obtained by fitting the proposed model using the FEA data shown in Fig. 3. The fitted parameters are physically reasonable, and they are consistent with the operating point. For comparison, the parameters obtained by fitting the conventional space-vector model[1] to the frequency-response data shown in Fig. 4 are also given; the only operating-point quantities used in the fitting were the angular frequencies ω_{s0} and ω_{r0} [13]. The fitted magnetizing inductance L_{m0} of the space-vector model is between the inductances L_{m0} and L_{mt0} of the proposed model. The single-cage model including the saturation was also investigated. It was noticed that the single-cage model can be used only at very low frequencies (ω less than 0.1 p.u.) in the case of this 37-kW machine.

Fig. 5(a) depicts the admittances of Fig. 3 at the frequency $\omega = 0.1$ p.u. as a function of the angle ϑ_0 of the coordinate system. When the angle is $\vartheta_0 = 0$, the coordinates are fixed to the operating-point stator voltage. Due to saturation, the admittance matrix depends on the angle ϑ_0.

The impulse excitation was also applied to the rotor position angle while keeping the supply voltage constant. In this case, the response of electromagnetic torque was studied. The transfer function from the rotor speed to the electromagnetic torque was investigated by applying an impulse to the speed

---

[1]The space-vector model equals the proposed model when $L_{mt0} = L_{m0}$, $L_{r\sigma t0} = L_{r\sigma 0}$, and $L_{t0} = 0$ are fixed.
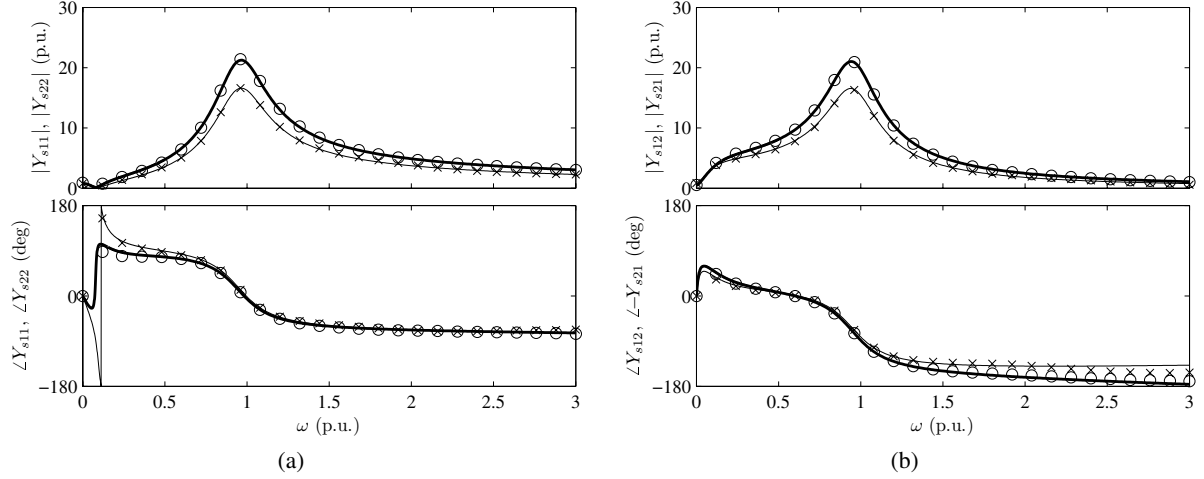
Fig. 3: Admittances from FEA (circles and crosses) and from fitted model (27): (a) $Y_{s11}(j\omega)$ shown by thick line and circles, $Y_{s22}(j\omega)$ shown by thin line and crosses; (b) $Y_{s12}(j\omega)$ shown by thick line and circles, $Y_{s21}(j\omega)$ shown by thin line and crosses. Coordinates are fixed to $\boldsymbol{u}_{s0}$. In the case of no saturation, conditions $Y_{s11}(j\omega) = Y_{s22}(j\omega)$ and $Y_{s12}(j\omega) = -Y_{s21}(j\omega)$ would hold.

Table I: Fitted per-unit parameters. Parameters $L_{s\sigma} = 0$ and $L_{r\sigma 10} = 0$ were fixed.

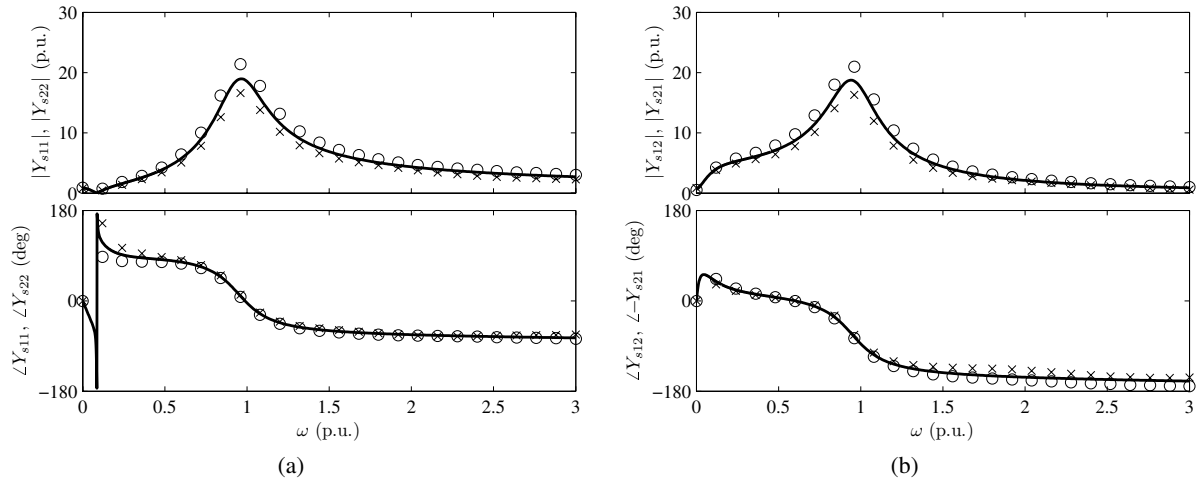|	Proposed model	Space-vector model
R_s	0.028	0.028
R_{r1}	0.102	0.106
R_{r2}	0.034	0.029
L_{m0}	2.683	1.777
$L_{r\sigma 0}$	0.175	0.133
$L_{r\sigma 20}$	0.106	0.112
L_{mt0}	1.530	
$L_{r\sigma t0}$	0.117	
L_{t0}	-0.089	

Fig. 4: Admittances from FEA (circles and crosses) and from fitted space-vector model (line): (a) $Y_{s11}(j\omega)$ shown by circles, $Y_{s22}(j\omega)$ shown by crosses; (b) $Y_{s12}(j\omega)$ shown by circles, $Y_{s21}(j\omega)$ shown by crosses. Coordinates are fixed to $\boldsymbol{u}_{s0}$. Only one line can be seen since $Y_{s11}(j\omega) = Y_{s22}(j\omega)$ and $Y_{s12}(j\omega) = -Y_{s21}(j\omega)$ hold for space-vector model.
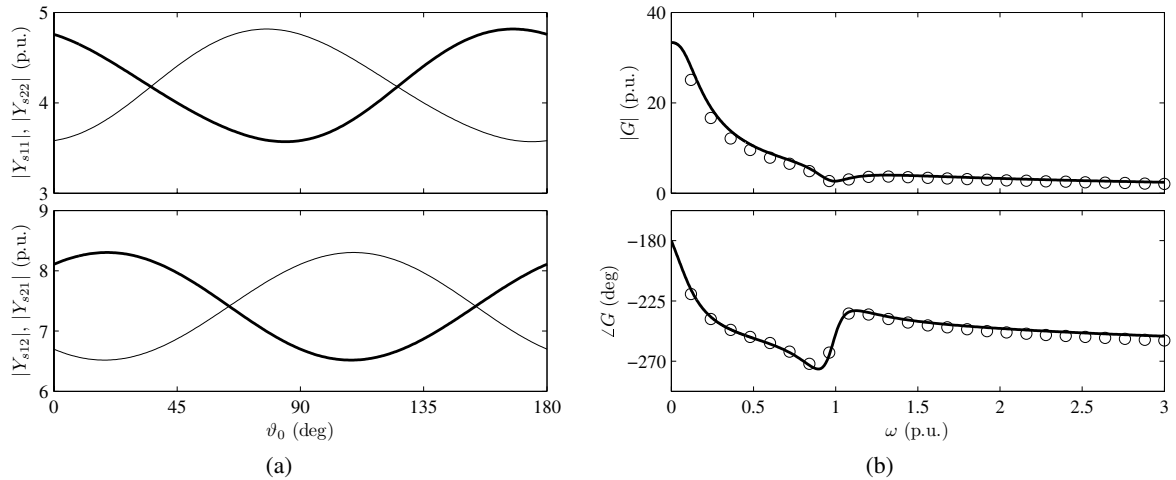
Fig. 5: (a) Admittances of Fig. 3 at $\omega = 0.5$ p.u. as a function of the angle ϑ_0 of vector $\boldsymbol{u}_{s0}$. In the case of no saturation, the admittances are independent of ϑ_0. (b) Frequency response $G(j\omega)$. The solid line is obtained using (29) and the fitted parameters corresponding to Fig. 3. Circles are calculated based on the speed-impulse test carried out in FEA.

while the motor was supplied by a sinusoidal voltage in time-stepping FEA. Transforming this data into the frequency domain, the frequency response shown by the circles in Fig. 5(b) is obtained. For comparison, the frequency response was calculated using (29) and the parameter values obtained by fitting the admittance matrix (Table I). This transfer function is shown in Fig. 5(b) by the solid line. It can be observed that the proposed model fits very well to the data from the speed impulse test. Hence, the fitted parameter values—obtained from the voltage impulse tests—are consistent with the data from the speed impulse test.

5   Conclusions

The magnetic saturation and the skin effect of rotor bars can be taken into account when deriving a small-signal model for the induction machine. The proposed model fulfills the reciprocity conditions, and it can be applied to parameter identification and to the analysis and development of flux angle estimation methods. Furthermore, the small-signal relationship between the rotor speed and the electromagnetic torque—needed if torsional dynamics are analyzed—can be evaluated. As an application example, the machine parameters were identified using the data obtained from time-stepping finite-element analysis. The proposed model fits well to the data from FEA, and the parameters identified are physically reasonable.

References

[1] A. Yahiaoui and F. Bouillault, "Saturation effect on the electromagnetic behaviour of an induction machine," *IEEE Trans. Magn.*, vol. 31, no. 3, pp. 2036–2039, May 1995.

[2] C. Gerada, K. Bradley, M. Sumner, and P. Sewell, "Evaluation and modelling of cross saturation due to leakage flux in vector controlled induction machines," in *Proc. IEEE IEMDC'03*, vol. 3, Madison, WI, June 2003, pp. 1983–1989.

[3] M. Hinkkanen, A.-K. Repo, and J. Luomi, "Influence of magnetic saturation on induction motor model selection," in *Proc. ICEM'06*, Chania, Greece, Sept. 2006, CD-ROM.

[4] P. L. Jansen and R. D. Lorenz, "Transducerless field orientation concepts employing saturation-induced saliences in induction machines," *IEEE Trans. Ind. Appl.*, vol. 32, no. 6, pp. 1380–1393, Nov./Dec. 1996.

[5] F. Blaschke, J. van der Burgt, and A. Vandenput, "Sensorless direct field orientation at zero flux frequency," in *Conf. Rec. IEEE-IAS Annu. Meeting*, vol. 1, San Diego, CA, Oct. 1996, pp. 189–196.

[6] M. L. Aime, M. W. Degner, and R. D. Lorenz, "Saturation measurements in AC machines using carrier signal injection," in *Conf. Rec. IEEE-IAS Annu. Meeting*, vol. 1, St. Louis, MO, Oct. 1998, pp. 159–166.

[7] J. A. A. Melkebeek, "Magnetising-field saturation and dynamic behaviour of induction machines; Part I: Improved calculation method for induction-machine dynamics," *IEE Proc. B, Electr. Power Appl.*, vol. 130, no. 1, pp. 1–9, Jan. 1983.

[8] R. C. Healey, S. Williamson, and S. C. Smith, "Improved cage rotor models for vector controlled induction motors," *IEEE Trans. Ind. Appl.*, vol. 31, no. 4, pp. 812–822, July/Aug. 1995.

[9] E. Levi, "Main flux saturation modelling in double-cage and deep-bar induction machines," *IEEE Trans. Energy Convers.*, vol. 11, no. 2, pp. 305–311, June 1996.

[10] S. D. Sudhoff, D. C. Aliprantis, B. T. Kuhn, and P. L. Chapman, "An induction machine model for predicting inverter–machine interaction," *IEEE Trans. Energy Convers.*, vol. 17, no. 2, pp. 203–210, June 2002.

[11] N. A. Retiere and M. Ivanes, "An introduction to electric machine modeling by systems of non integer order," *IEEE Trans. Energy Convers.*, vol. 14, no. 4, pp. 1026–1032, Dec. 1999.

[12] A. Arkkio, "Analysis of induction motors based on the numerical solution of the magnetic field and circuit equations," Ph.D. dissertation, Dept. Elect. Commun. Eng., Helsinki Univ. Tech., Espoo, Finland, Dec. 1987. [Online]. Available: http://lib.tkk.fi/Diss/198X/isbn951226076X/

[13] A.-K. Repo and A. Arkkio, "Numerical impulse response test to identify parametric models for closed-slot deep-bar induction motors," *IET Electr. Power Appl.*, vol. 1, no. 3, pp. 307–315, May 2007.

[14] L. O. Chua, "Dynamic nonlinear networks: State-of-the-art," *IEEE Trans. Circuits Syst.*, vol. CAS-27, no. 11, pp. 1059–1087, Nov. 1980.

[15] P. W. Sauer, "Constraints on saturation modeling in ac machines," *IEEE Trans. Energy Convers.*, vol. 7, no. 1, pp. 161–167, Mar. 1992.

[16] A. Tabesh and R. Iravani, "Frequency-response analysis of torsional dynamics," *IEEE Trans. Power Syst.*, vol. 19, no. 3, pp. 1430–1437, Aug. 2004.

[17] L. Harnefors, "Analysis of subsynchronous torsional interaction with power electronic converters," *IEEE Trans. Power Syst.*, vol. 22, no. 1, pp. 305–313, Feb. 2007.

[18] A. Repo and A. Arkkio, "Numerical impulse response test to estimate circuit-model parameters for induction machines," *IEE Proc. Electr. Power Appl.*, vol. 153, no. 6, pp. 883–890, Nov. 2006.

[19] K. Price, R. Storn, and J. Lampinen, *Differential Evolution: A Practical Approach to Global Optimization*.   Berlin, Germany: Springer, 2005.

[20] F. Córcoles, J. Pedra, M. Salichs, and L. Sainz, "Analysis of the induction machine parameter identification," *IEEE Trans. Energy Convers.*, vol. 17, no. 2, pp. 183–190, June 2002.